Co-immobilized Alcohol Dehydrogenase and Glucose Dehydrogenase with Resin Extraction for Continuous Production of Chiral Diaryl Alcohol

Jieyu Zhou
Jiangnan University
Yanfei Wu
Jiangnan University
Qingye Zhang
Jiangnan University
Guochao Xu
Jiangnan University
YE NI (yni@jiangnan.edu.cn)
Jiangnan University https://orcid.org/0000-0003-4887-7517

Research Article

Keywords: flow reaction, alcohol dehydrogenase, co-immobilization, diaryl ketone, in situ recovery

Posted Date: February 17th, 2021

DOI: https://doi.org/10.21203/rs.3.rs-238951/v1

Version of Record: A version of this preprint was published at Applied Biochemistry and Biotechnology on April 7th, 2021. See the published version at https://doi.org/10.1007/s12010-021-03561-5.

Co-immobilized Alcohol Dehydrogenase and Glucose Dehydrogenase with Resin Extraction for Continuous Production of Chiral Diaryl Alcohol

*Jieyu Zhou, Yanfei Wu, Qingye Zhang, Guochao Xu, Ye Ni**

Key laboratory of industrial Biotechnology, Ministry of Education, School of Biotechnology, Jiangnan University, Wuxi 214122, Jiangsu, China.

*Corresponding author

Tel/Fax: +86-510-85329265

Email: yni@jiangnan.edu.cn

Abstract

Ni^{2+}-functionalized porous ceramic/agarose composite beads (Ni-NTA Cerose) can be used as carrier materials to immobilize enzymes harboring a metal affinity tag. Here, a 6×His-tag fusion alcohol dehydrogenase Mu-S5 and glucose dehydrogenase from *Bacillus megaterium* (*Bm*GDH) were co-immobilized on Ni-NTA Cerose to construct a packed bed reactor (PBR) for the continuous synthesis of the chiral intermediate (*S*)-(4-chlorophenyl)-(pyridin-2-yl) methanol [(*S*)-CPMA]. NADPH recycling and *in situ* product adsorption was achieved simultaneously by assembling a D101 macroporous resin column after the PBR. Using an optimum enzyme activity ration of 2:1 (Mu-S5: *Bm*GDH) and hydroxypropyl-*β*-cyclodextrin as co-solvent, a space-time yield of 1,560 g/(L·d) could be achieved in the first three days at a flow rate of 5 mL/min and substrate concentration of 10 mM. With simplified selective adsorption and extraction procedures, (*S*)-CPMA was obtained in 84% isolated yield.

Keywords:

flow reaction; alcohol dehydrogenase; co-immobilization; diaryl ketone; *in situ* recovery

Abbreviations:

ADH, alcohol dehydrogenase; GDH, glucose dehydrogenase; FDH, formate dehydrogenase; CPMK, (4-chlorophenyl)(pyridine-2-yl)ketone; (*S*)-CPMA, (*S*)-(4-Chlorophenyl)-(pyridin-2-yl) methanol; DNPH, 2,4-dinitrophenylhydrazine; PBR, packed bed reactor; Cerose, ceramic/agarose composite beads

Introduction

In comparison to batch reactions, flow reactions are relatively new for biocatalytic preparation of value-added chemicals and active pharmaceutical ingredients, such as (*S*)-1-phenylethanol, (*R*)-flurbiprofen, fatty acid methyl esters etc. [1, 2]. In a flow reaction, fluid containing substrates is pumped to the reactor to produce a product stream [3-6]. When a flow process is applied to biocatalysis, it can be performed by using immobilized cells or enzymes [7-11]. As a continuous process, flow reactions have advantages of improved productivity, safety, ease of modifying scale, and are especially useful for reactions with substrate/product inhibitory issues [12]. Additionally, downstream processing can become facile when using immobilized biocatalysts [13].

For coupling or multienzymatic reaction systems, co-immobilization is an ideal strategy. Co-immobilization could facilitate *in situ* removal of by-products, and is essential for reactions that require cofactor regeneration [14, 15]. Co-immobilization of the main and regeneration enzymes can also facilitate the mobility of the co-factor between two enzymes. Therefore, it is critical to develop immobilization strategies favorable for preserving the activity of all involved enzymes. Additionally, the distribution of the enzyme on the support surface has a profound impact on the enzyme's overall biocatalytic activity [16]. Guián's group has developed an elegant approach in which they co-immobilize the main and recycling dehydrogenases on the same agarose-type support (activated with glyoxyl groups and metal chelates) [17]. Recently, this approach was adopted in a co-immobilized glycosyltransferase/sucrose synthase catalyzed

system for NDP-glucose recycling [18].

Immobilized metal affinity chromatography (IMAC) has also been regarded as a potential strategy for enzyme co-immobilization. The IMAC strategy relies on coordination bonds between transition metal ions (such as Ni^{2+}, Cu^{2+}, Zn^{2+}, and Co^{2+}) and certain amino acids (such as His, Cys, and Trp) [19]. Co-expression of special fusion peptides results in specific coordinations between metal ions and proteins, giving advantages such as easy operation, target-specific purification, low activity loss, and recyclable carrier materials [20-24]. His-tag is one of the most popular fusion peptide for IMAC [25, 26]. In Böhmer and coworkers' study, a 6×His-tag fusion alcohol dehydrogenase (ADH) and amine dehydrogenase (AmDH) were co-immobilized on commercial metal-ion affinity glass beads EziG to produce chiral amine in batch reactions [27]. Additionally, Heli-tag, a metal-binding site (His-Ile-His-Asn-Leu-Asp-Cys-Pro-Asp-Cys) found in ATPase 439 from *Helicobacter pylori*, was identified to have strong metal affinity [28, 29]. The Heli-tag was reported to exhibit higher affinity than the 6×His-tag and has been successfully used for D-amino acid oxidase immobilization to obtain improved operational stability [30].

Notably, the co-immobilization strategies discussed above have mainly been applied in batch reactions. Additional aspects need to be considered when adopting co-immobilized enzymes in continuous reactions, such as operational stability and cofactor-recycling under flow mode. In a study by Dall'Oglio et al., chemical anchoring was adopted for co-immobilization of ADH and GDH to construct a continuous flow reactor. The stability of this system proved to be excellent during a 15-day operation

run at a flow rate of 50 μL/min [31]. Peschke et al. constructed an all-enzyme hydrogel consisting of ADH and GDH using a self-assembling strategy, in which a stable bioconversion was operated for over 6 days at a flow rate of 10 μL/min [32]. However, activity loss caused by covalent anchors and insufficient structural rigidity of the all-enzyme hydrogel restricted the flow rate of the continuous reaction. Moreover, a continuous flow of cofactor was required in both studies. A regenerative electrochemical method [33, 34] and cofactor immobilization [35] have been reported for cofactor recycling in continuous flow biocatalysis; however, these studies were limited by complex immobilization procedures or reusability of immobilized carriers [36]. Given these limitations, we proposed a co-immobilization strategy for $NADP^+$/NADPH reutilization and regeneration with *in situ* product extraction in a continuous reaction.

In this study, a non-ionic adsorptive resin was used for $NADP^+$ recycling due to its specific adsorption of non-polar or low-polar organic compounds from aqueous solutions. Herein, we designed an $NADP^+$/NADPH regeneration strategy for a continuous flow reaction catalyzed by co-immobilized ADH/GDH. The asymmetric reduction of (4-chlorophenyl)(pyridine-2-yl)ketone (CPMK) catalyzed by Mu-S5 (a mutant of *Kp*ADH from *Kluyveromyces polyspora*) [37, 38] was investigated as the model reaction. The chiral product (*S*)-(4-Chlorophenyl)-(pyridin-2-yl) methanol [(*S*)-CPMA] is an important intermediate for synthesizing the antiallergy drug bepotastine [38, 39]. *Bm*GDH from *Bacillus megaterium* was used for NADPH regeneration. The 6×His-tagged Mu-S5 and *Bm*GDH were co-immobilized on nickel-nitrilotriacetic acid-

functionalized porous ceramic/agarose composite beads (Ni-NTA Cerose) to construct a packed bed reactor (PBR), which was followed by a D101 macroporous resin column. The feasibility of the proposed flow reaction process was validated by continuous synthesis and *in situ* recovery of (*S*)-CPMA.

Materials and Methods

Microorganisms and chemicals

Recombinant *E. coli BL21* (DE3) strains harboring pET28-Mu-S5 and pET28-*Bm*GDH with *N*-terminal 6×His-tag were constructed in a previous study [38]. Ni-NTA Cerose was purchased from Qianchun Bio (Yancheng, China). Macroporous resins of D101 and XDA-1 and chelating rein IRC-748 were purchased from Lebiochem, Co. Ltd. (Xian, China). (4-Chlorophenyl)(pyridin-2-yl)methanone (CPMK) and all other reagents and solvents of analytical grade and biochemical reagents were obtained from Sinopharm Chemical Reagent Co. Ltd. (Shanghai, China).

Construction of N-terminal Heli-tagged Mu-S5

Plasmid pET28-Helitag-Mu-S5 was constructed by replacing the N-terminal 6×His-tag sequence in pET28-Mu-S5. Plasmid pET28-Mu-S5 was used as the template, 6×His-tag at N-terminal was replaced with Heli-tag by whole-plasmid PCR using KOD-Plus-Neo DNA polymerase purchased from Toyobo (Osaka, Japan). The following upstream and downstream primers were used:

Heli-tag-F:

CATATTCATAATCTTGATTGTCCTGATTGTAGCAGCGGCCTGGTG

Heli-tag-R:

ACAATCAGGACAATCAAGATTATGAATATGGCTGCTGCCCATGGT

The PCR protocol was as follows: 95°C for 2 min, followed by 15 cycles of 94°C for 30 s, 55°C for 30 s, and 68°C for 2.5 min. After *Dpn* I digestion at 37°C for 30 min, the PCR products were transformed into competent *E. coli* BL21 (DE3) cells and plated onto Luria-Bertani agar plates supplemented with 50 μg/mL kanamycin.

Screening of supporting materials for enzyme immobilization

Preparation of the NTA Cerose column

Each column (Φ=72 mm, h=24 mm) was packed with 1 mL of NTA Cerose and washed with 10 mL of deionized water followed by a solution of $NiSO_4$ or $MnCl_2$ (10 mL, 100 mM). The columns were then washed with 10 mL of deionized water to remove the unbound metal ions, and equilibrated with 100 mM potassium phosphate buffer (pH 7.5). A ten-fold scale-up was used for the 10 mL Ni-NTA column.

Preparation of reaction solution

Solution A: For 1 mL PBR, a mixture solution containing 20% ethanol (v: v), 2 mM CPMK, 2 mM glucose and 2 mM $NADP^+$ was prepared with 100 mM sodium phosphate buffer at pH 7.0. The mixture was warmed to 30°C before use.

Solution B: For 10 mL PBR (after optimization); a mixture solution containing 20 mM hydroxypropyl-beta-cyclodextrin (HP-β-CD), 10 mM glucose and 10 mM $NADP^+$ was prepared with 100 mM Tris-HCl buffer at pH 7.5. The mixture was incubated at 30°C

for 1 h, and then CPMK (1M in ethanol) was added to a final concentration of 10 mM.

Determination of the amount of immobilized enzyme and dilution rate

Mn-NTA and Ni-NTA Creose columns (1-mL) were prepared as described above. First, Mu-S5 was purified by Ni affinity chromatography and desalinated by ultrafiltration centrifugation. The resultant purified Mu-S5 was obtained with specific activity of 6.64 U/mg (**Table S1**), and then diluted to around 10 U/mL (the actual value was determined to be 11.7 U/mL).

The amount of immobilized enzyme was measured by calculating the difference in enzyme activity between inflows and outflows. It is presumed that saturation adsorption was reached when total activity in outflows was 10% of the initial activity. The enzyme activities of inflows and outflows were measured following assay method described in analysis methods. The total activity of the immobilized enzyme was equal to the difference in total activity between inflows and outflows, and the amount of immobilized enzyme could be calculated by dividing by the specific activity of Mu-S5 (6.64 U/mg). The detailed data can be found in supplemental data (**Table S2**).

Dilution rate: According to the optimized results, the enzyme loading was 20 mg protein per mL of Ni-NTA Cerose (eg. 16.7 mg protein/g Ni-NTA Cerose). Thus, 14.11 mg of purified Mu-S5 (94 U) and 5.89 mg of purified *Bm*GDH (47 U) were needed to construct a 1-mL PBR based on Ni-NTA/Mn-NTA Cerose. For operational convenience, 10 mg/mL solutions of both Mu-S5 and *Bm*GDH were prepared, corresponding to 1.41 mL and 0.596 mL loading volume, respectively. Then, a peristaltic pump was used to pump the reaction solution through the reactor at flow

rates of 0.2, 0.4, 0.6, 0.8, and 1.0 mL/min. For a 10-mL Ni-NTA PBR, 141.1 mg (940 U) of Mu-S5 and 58.9 mg (470 U) of *Bm*GDH were mixed and loaded, and the flow rates were set at 2.0, 4.0, 6.0, 8.0, and 10 mL/min. All of the post-column effluents were collected separately and detected by HPLC.

$$\text{Dilution rate} = \frac{\text{Volumetric flow rate (mL/min)}}{\text{Reactor volume (mL)}}$$

Analysis methods

Enzymatic activity assay

The activity of Mu-S5 and *Bm*GDH was spectrophotometrically determined according to the changes in absorption of NADPH or $NADP^+$ at 340 nm and 30°C with a UV–Vis spectrophotometer using a molar extinction coefficient of 6,220 $M^{-1}cm^{-1}$. For Mu-S5, the assay mixture contained 1.0 mM CPMK, 1.0 mM NADPH, and a proper amount enzyme in PBS buffer (100 mM, pH 7.0). For *Bm*GDH, the assay mixture contained 1 mM D-glucose, 1 mM $NADP^+$, and 10 μL enzyme in PBS buffer (100 mM, pH 7.0). One unit of activity was defined as the amount of enzyme required for the depletion or production of 1.0 μmol of NADPH under the aforementioned conditions.

HPLC analysis

The substrate conversion and *ee* value was determined using an Agilent 1100 HPLC system (USA) equipped with a Chiralcel OB-H column (0.46 mm × 250 mm, 5 μm, Diacel, Japan). The HPLC was performed at 254 nm using hexane:ethanol (95:5, v/v) as eluent at a flow rate of 0.8 mL/min.

Activity recovery of immobilized Mu-S5

190 Since spectrophotometric determination was not applicable for immobilized Mu-S5,
191 the initial velocities of all entries were calculated using the substrate conversion from
192 the first 10 min (substrate conversion < 20%) using an HPLC assay.
193 A purified Mu-S5 solution of 10 U/mL was prepared as described above. The Mu-S5
194 solutions (40 mL) were loaded on 1 mL Ni-NTA and Mn-NTA PBR columns,
195 respectively. Enzymatic activity of inflows was performed in a 2 mL reaction mixture
196 consisting of 10 mM CPMK, 10 mM NADPH, and 250 μL inflows in 100 mM PBS
197 (pH 7.0) at 30°C and 200 rpm for 10 min (**Fig. S1 & Table S3**).
198 The outflows were collected and the enzymatic activity was determined in a 2 mL
199 reaction mixture consisting of 10 mM CPMK, 10 mM NADPH, and 1 mL outflows in
200 100 mM PBS (pH 7.0) at 30°C and 200 rpm for 10 min (**Fig. S2 & Table S4**).
201 The activity of immobilized Mu-S5 was determined as follows. Weight (in gram) rather
202 than volume (in mL) was used to quantify immobilized Mu-S5. The total weights of 1
203 mL of immobilized enzymes (Mn-NTA and Ni-NTA Creose) were measured to be 1.23
204 and 1.20 g, respectively. Immobilized Mu-S5 was placed in a beaker containing 9 mL
205 100 mM PBS (pH 7.0) buffer. After mixing, 100 μL homogenized solution was
206 transferred into 2.0 mL tubes followed by centrifugation. The liquid was then carefully
207 removed, and the immobilized Mu-S5 were weighed. The activity of immobilized Mu-
208 S5 was determined in a 2 mL reaction mixture consisting of 10 mM CPMK, 10 mM
209 NADPH, and about 0.01g of immobilized Mu-S5 in 100 mM PBS (pH 7.0) at 30°C and
210 200 rpm for 10 min (**Fig. S3 & Table S5**). The data are summarized in **Table S6**.
211 $$\text{Activity recovery} = \frac{\text{Activity of immobilized enzyme}}{\text{Inflows activity-Outflows activity}} \times 100\%$$

212 ***2,4-Dinitrophenylhydrazine (DNPH) assay***

213 DNPH (2,4-dinitrophenylhydrazine) is a reagent used to detect the carbonyl of ketone
214 or aldehyde functional groups. In this study, the formation of red
215 dinitrophenylhydrazone with CPMK and DNPH substrates can be regarded as a
216 positive result. First, DNPH was dissolved at 20 mM in ethanol containing 3% sulfuric
217 acid and stored in darkness. Then, the chromogenic reaction was performed by addition
218 of 100 μL of the DNPH solution into 100 μL of effluent (after packed bed reactor).
219 After standing for 15 min at 30°C, 1 mL of KOH (0.5 M) was added, and the absorbance
220 of the solution was determined at 500 nm by a microplate reader (Biotek, USA).
221 Samples without CPMK were used as the control.

222

223 **Bio-reduction catalyzed by immobilized enzyme**

224 ***Optimal pH and temperature***

225 Substrate conversion was performed in a 5-mL mixture containing Mu-S5 and *Bm*GDH
226 (2 U each), 50 mM CPMK, and 50 mM glucose. The optimal pH of the reaction was
227 determined by measuring the substrate conversion in the following buffers: sodium
228 citrate-citric acid buffer (SCC buffer, pH 5.0–6.0, 100 mM), sodium phosphate buffer
229 (pH 6.0–8.0, 100 mM), and Tris-HCl (pH 7.5–9.0, 100 mM). The optimal temperature
230 was determined by measuring substrate conversion at 25–40°C.

231 ***Optimal ratio of Mu-S5 and BmGDH***

232 A total dry mass of 2 mg purified Mu-S5 and *Bm*GDH were mixed at activity ratios of
233 10:1 to 1:10. The reaction mixture containing 100 mM CPMK, 100 mM glucose,

234 premixed solutions of Mu-S5 and *Bm*GDH, and 100 mM Tris-HCl (pH 7.5) in a final
235 volume of 5 mL, was conducted at 30°C for 30 min. The substrate conversion was
236 analyzed by HPLC.

237 ***Effect of various co-solvents***

238 In the pre-experiments, 10 mM CPMK was dissolved in different co-solvents. A mother
239 solution of CPMK (1.0 M) was prepared in ethanol by heating. Different amounts of
240 co-solvents were added into 10 μL of the CPMK mother solution (1.0 M), then different
241 volumes of water were added to a final volume of 1 mL (**Table S7 & S8**). According
242 to preliminary results, 5% Tween 80, 2.5% Triton X-100, and 20–40 mM HP-*β*-CD
243 were tested as co-solvents. Substrate conversion was performed in a 5-mL mixture
244 containing 0.2 U of Mu-S5 and 0.1 U of *Bm*GDH, 10 mM glucose, and 10 mM CPMK.
245 The substrate conversion was analyzed by HPLC.

246

247 **Extraction with macroporous resins**

248 ***Static adsorption/desorption rate of macroporous resins toward CPMA***

249 Adsorption rate: Substrate CPMK in Solution B was replaced with the product (*S*)-
250 CPMA to prepare Solution C. A mass of 0.5 g resin D101 or XDA-1 was added into 10
251 mL of Solution C; the adsorption process was then carried out at 30°C and 150 rpm for
252 4 h, and the non-adsorbed (*S*)-CPMA was analyzed by HPLC.

253 $$\text{Adsorption rate} = \frac{\text{Initial concentration-Residual concentration}}{\text{Initial concentration}} \times 100\%$$

254 Desorption rate: The 0.5 g masses of resin D101 or XDA-1 that had adsorbed (*S*)-
255 CPMA were washed with water and filtered on a Buchner funnel. A volume of 10 mL

ethanol or ethyl acetate was added, and the desorption process was carried out at 30°C and 150 rpm for 4 h. The concentration of (*S*)-CPMA in the desorbing agent was analyzed by HPLC.

$$\text{Desorption rate} = \frac{\text{Concentration in the desorbing agent}}{\text{Initial concentration}} \times 100\%$$

Adsorption capacity of macroporous resins toward $NADP^+$

A mass of 0.5 g resin D101 or XDA-1 was added to 10 mL of solution containing 10 mM $NADP^+$. The adsorption process was carried out at30°C and 150 rpm for 4 h and the absorption capacity was determined using an EnzyChrom $NADP^+$/NADPH assay kit from BioAssay Systems (Hayward, CA).

Continuous flow reaction in a 10-mL PBR

A 12-mL polypropylene column was packed with 10 mL of Ni-NTA Cerose to prepare a PBR. A total of 200 mg of purified enzyme was loaded (141.1 mg Mu-S5 (940 U) and 58.9 mg *Bm*GDH (470 U)), and the enzyme loading was 20 mg protein/mL Ni-NTA Cerose (eg. 16.7 mg protein/g Ni-NTA Cerose). For operational convenience, 50 mg/mL solutions of both Mu-S5 and *Bm*GDH were prepared, corresponding to 5.08 mL and 1.99 mL loading volumes, respectively. A peristaltic pump was used to pump Solution B through the PBR at 5 mL/min. A glass column filled with 28 g (40 mL) of resin D101 was connected to the PBR to extract CPMA from the effluent of the PBR. A total of 4 L of reaction solution was prepared as described above. To ensure the continuity of the process, the 4 L initial reaction solution was divided into two portions (2 L each) for rotation. According to the dynamic adsorption capacity of macroporous

resin D101, 5 columns (40 mL) filled with D101 were required to adsorb (*S*)-CPMA from 2 L of effluent. In this study, a fresh D101 column was changed every 80 min. Notably, D101 resin is reproducible and recyclable. After 400 min, 2 L of effluent solution was collected, and 2 mL CPMK solution (dissolved in ethanol at 1 M) was added as reaction solution for recycling. Meanwhile, the resin 101 that adsorbed (*S*)-CPMA in each column was collected and filtered with a Buchner funnel. A double volume (80 mL) of ethyl acetate was added, and the desorption process was carried out at 30°C and 150 rpm for 4 h. The product (*S*)-CPMA was concentrated by rotary evaporation.

The space-time-yield (STY) was defined as the mass of (*S*)-CPMA produced per milliliter of PBR enzyme per day.

$$\text{STY}= \frac{\text{Amount of (}S\text{)-CPMA (g)}}{\text{Volume of PBR (L)}\times\text{Reaction time (d)}}$$

Treatment of column packing for recovery and reuse

After each batch process, the immobilized Ni-NTA Cerose was washed with 10 column volumes of 50 mM EDTA and water sequentially. After 30 min incubation with a solution of 100 mM $NiSO_4$, the column was washed with 10 column volumes of water, and then reused for the next batch.

For the product adsorbent column, (*S*)-CPMA was collected by soaking with ethyl acetate, then the D101 macroporous resin was sequentially washed using a Buchner funnel with 2 column volumes of the following: a solution containing 95% ethanol, water, and 3% HCl; water (rinsed to neutral); a 3% NaOH solution; water (rinsed to

neutral).

Results and discussion

Device for enzyme immobilization and product recovery

For continuous synthesis of (*S*)-CPMA, a prototype combined device consisting of four main parts was designed (**Fig. 1**), including a bottle of flow reaction solution (containing dissolved CPMK, $NADP^+$, and glucose), a PBR containing Ni-NTA Cerose with immobilized Mu-S5 and *Bm*GDH, a macroporous resin column for adsorbing hydrophobic products, and a beaker for effluent recovery. When the reaction solution flowed through the PBR, the ketone substrate CPMK was reduced into the corresponding chiral alcohol (*S*)-CPMA. After that, the hydrophobic (*S*)-CPMA would be adsorbed by the resin column, whereas the effluent solution containing residual water-soluble NAD(P)H/$NAD(P)^+$ and by-product gluconate would be collected for recovery. After replenishing CPMK and glucose, the effluent solution could be reused as reaction solution. The post-column samples of the PBR and the resin column were determined by using a previously established DNPH assay [37] to ensure complete bio-reduction and adsorption. When the resin column reached saturation, it could easily be replaced with a new one, and the adsorbed (*S*)-CPMA could be separated from the resin by static or dynamic elution. This operation mode not only avoids the emulsification issue caused by extraction with organic solvents in biocatalytic reaction system, but also allows for the reuse of expensive cofactors. Moreover, Ni-NTA Cerose could be recycled and reused by treatment with EDTA and $NiSO_4$ solutions after each batch. For

the product adsorbent column, D101 macroporous resin is also recyclable and can be reused by treatment with dilute acid and alkali solutions. The whole process is simple and easy to operate with low material and downstream costs. Optimization of reaction conditions was performed to verify the feasibility of the continuous reaction process.

Screening of supports for the immobilization of Mu-S5 and *Bm*GDH

Immobilized metal affinity chromatography (IMAC) is commonly used for His-tagged protein purification and can also be applied to the immobilization of enzymes [25]. Herein, a commercially available NTA Cerose was chosen as the immobilization carrier material. Compared with the NTA agarose (0.05 Mpa/cm) commonly used in purification, NTA Cerose (1 Mpa/cm) possesses a stronger stability under system pressure and can withstand relatively higher flow rates. Ni^{2+} and Mn^{2+} were selected due to their positive effects on the catalytic activity of Mu-S5 (104% for Ni^{2+} and 116% for Mn^{2+}) (**Fig. 2A**). After immobilization, protein loading per gram carrier was calculated to be 61.9 mg for Ni-NTA Cerose and 42.2 mg for Mn-NTA Cerose (**Table S2**). Additionally, Ni-NTA Cerose and Mn-NTA Cerose maintained 58.0% and 66.4% relative catalytic activity compare with that of free enzyme in shake flasks, respectively (**Table S6**).

The dilution ratio was defined as the reactor volume divided by the volumetric flow rate of substrate, and it was used to evaluate the reactor performance. For Ni-NTA Cerose immobilized Mu-S5, the substrate conversion remained over 99% with increased substrate flow rate, whereas a consistent decline of conversion was observed

for Mn-NTA Cerose. The conversion decreased to less than 50% at a flow rate of 1 mL/min for Mn-NTA (**Fig. 2B**). Due to the larger ionic radius of the Mn^{2+} ion (91 nm) compared to the Ni^{2+} ion (73 nm), the metal coordination bond strength of Ni^{2+} is stronger than that of Mn^{2+}. This difference in coordination bond strength is likely responsible for the poor performance of Mn-NTA. Notably, no protein leaching was detected at dilution rates of 0.2–1.0 min^{-1} as evaluated by a Bradford assay. Therefore, insufficient enzyme immobilized on Mn-NTA is likely responsible for the low conversion. To further reduce the cost, a cheaper chelating resin IRC-748 was functionalized with Ni^{2+} and employed for enzyme immobilization. However, activity above 85% was lost after immobilization due to the poor biocompatibility of the resin. Therefore, Ni-NTA Cerose was selected for protein immobilization.

Comparison of *6*×His-tag and Heli-tag in protein immobilization

In addition to the 6×His- tag, the Heli-tag fusion peptide with higher affinity was attempted for immobilization [28, 29]. Since the C-terminal portion of Mu-S5 is buried and solvent inaccessible, the Heli-tag was fused to the N-terminal of Mu-S5.

The affinity of 6×His- and Heli-tagged Mu-S5 with Ni-NTA was compared under the same elution conditions (**Fig. 3**). The two fused Mu-S5s showed similar solubility as confirmed by SDS-PAGE. Both fusion proteins were barely detected in the flow-through (lane 3). The majority of the 6×His-tag fused Mu-S5 eluted at 100 mM imidazole, and some was eluted at 50 mM imidazole. (**Fig. 3B**). In contrast, almost all of the Heli-tag fused Mu-S5 was eluted at 20-50 mM imidazole (**Fig. 3 A**). After elution

366 with 50 mM imidazole, over 95% of enzymatic activity was lost with the of Heli-tag
367 fused Mu-S5, whereas only 3.9% activity loss was observed with the 6×His-tag fused
368 Mu-S5 (**Table S9**). It is speculated that the Heli-tag may not be fully exposed on the
369 surface of Mu-S5, which may affect the structure and conformation of the protein [40].
370 Collectively, the Heli-tag that has been proven to be effective in D-amino acid oxidase
371 immobilization [30] is not applicable for Mu-S5, and the 6×His-tag was used for
372 enzyme immobilization for further study.
373

374 **Optimization of reaction conditions of PBR**

375 The reaction conditions were optimized to obtain improved catalytic performance. The
376 pH, temperature, ratio of Mu-S5/*Bm*GDH, and co-solvent were optimized in shake
377 flasks, and the dilution rate was determined in a PBR. As shown in **Fig. 4A**, Mu-S5
378 showed optimal activity at pH 7.5 in Tris-HCl buffer. The optimal temperature of the
379 reaction was 30°C (**Fig. 4B**), and the reaction can be conveniently performed at room
380 temperature. Under the optimized pH and temperature, the highest conversion (75.1%)
381 was achieved using immobilized Mu-S5/*Bm*GDH at an activity ratio of 2:1 (**Fig. 4C**),
382 which may be related to the addition of an equal amount of glucose as co-substrate. As
383 there were not significant differences in the large-scale fermentation costs between Mu-
384 S5 and *Bm*GDH (**Table S1**), the optimized activity ratio of 2:1 is acceptable.
385 Additionally, an aqueous solution of the insoluble substrate CPMK should be prepared
386 for the continuous process. Several commonly used dispersants were screened, and a
387 10 mM aqueous solution of CPMK could be obtained when supplemented with 5%

Tween 80, 2.5% Triton X-100, and 20 mM hydroxypropyl-beta-cyclodextrin (HP-*β*-CD) in preliminary experiments (**Table S7 & S8**). **Fig. 4D** shows the effect of co-solvents on catalytic activity of immobilized Mu-S5, and a reaction system with the addition of 20% ethanol served as a control. A decrease in substrate conversions was observed when using Tween 80 and Triton X-100 as co-solvents, and this may be attributed to the disrupted protein conformation that results from the interactions between the nonionic surfactant and the hydrophobic region of the enzyme. Surprisingly, HP-*β*-CD not only improved the substrate solubility but also exhibited excellent biocompatibility. Benefiting from the hydrophilic exterior and hydrophobic interior structure of HP-*β*-CD, mass transfer was improved, and almost complete conversions were achieved with the addition of 20−40 mM HP-*β*-CD, whereas only 76.4% conversion was observed in the control reaction (20% ethanol). Finally, the dilution rate of 10 mL PBR (Φ=1.6 cm, h=5.5 cm) was determined under the optimized reaction conditions. As shown in **Fig. 4E**, the substrate conversion began to decrease when the volumetric flow rate of CPMK exceeded 6 mL/min, and only 93.1% conversion was detected at an increased flow rate of 10 mL/min without protein leaching. Considering possible damage to the immobilized materials and enzymes caused by the long-term continuous reaction, a volumetric flow rate of 5 mL/min was chosen.

Comparison of properties of D101 and XDA-1

Macroporous resins possess stable physical and chemical properties, and can be classified into three types: polar, non-polar, and weakly polar. According to the design,

410 the hydrophobic diaryl alcohol product is expected to be adsorbed whereas the water-
411 soluble cofactor should be recycled and reused for consecutive reaction cycles.
412 Therefore, two commonly used non-polar macroporous resins D101 and XDA-1 were
413 selected for (*S*)-CPMA enrichment (**Table S10**). The adsorption rate is an important
414 index to evaluate the adsorption performance of macroporous resins. As shown in **Table**
415 **1 & S11,** the two resins maintained almost the same adsorption capacity toward the
416 product (*S*)-CPMA. Resin XDA-1 with a larger surface area exhibited more than a 90%
417 static adsorption rate. The desorption rate of the two resins toward (*S*)-CPMA was also
418 compared (**Table S12**). Firstly, different proportions of recommended aqueous-ethanol
419 were used as washing solutions, however, only about 20% of the product could be
420 eluted even when pure ethanol (100%) was used. Then, ethyl acetate with lower polarity
421 was tested, and the desorption rate increased rapidly. In the case of D101, more than
422 95% of CPMA could be eluted with the addition of ethyl acetate, whereas only 82.6%
423 of CPMA could be eluted when XDA-1 was selected for extraction. Afterward, the
424 residual $NADP^+$ concentration was measured using an $NADP^+$/NADPH assay kit to
425 evaluate whether the selected resin could be used for coenzyme recycling. The results
426 showed that neither D101 nor XDA-1 could adsorb $NADP^+$ (**Table S13, Fig S4**). Thus,
427 D101 was selected as the supporting material in the extraction column due to the higher
428 desorption rate. Using a 40 mL column (Φ=1.6 cm, h=20 cm) filled with 28g of D101
429 resin, fractions were collected sequentially every 10 mL, and a trace amount of (*S*)-
430 CPMA was detected in the 47^{th} sample. The dynamic adsorption capacity of D101 was
431 calculated to be 36.3 mg/g, which is roughly equal to its static adsorption capacity (38.6

mg/g).

Asymmetric synthesis and in situ extraction of (*S*)-CPMA in a continuous device

Asymmetric synthesis of (*S*)-CPMA was carried out under optimized immobilization and reaction conditions. **Fig. 5** shows the conversion ratio of CPMK catalyzed by immobilized Mu-S5/*Bm*GDH in a 10-mL PBR. A complete conversion of CPMK was observed in the first 3 days followed by a gradual decline. When the reaction proceeded to day 4, an obvious red-brown color formed in DNPH assay, indicating an incomplete conversion of the ketone substrate. On day 7, only 54.3% conversion was observed by HPLC, and conversion continued to decreased sharply to 22.5% on day 8. In view of the negligible effect of the His-tag on protein structure, the insufficient stability of the Mu-S5 (half-life of 152 h at 30°C, **Fig. S5**) might be responsible for the decreased substrate conversion after day 3. Finally, the STY was calculated to be 1,560 g/(L·d) based on data from day 1 to 3. A total volume of 4 L initial reaction solution was recycled up to 6 times. After 400 min of reaction, the D101 resin in the first 5 adsorption columns was collected, and a total of 3.63 g (*S*)-CPMA with 84% isolated yield was obtained by ethyl acetate extraction.

Peschke et al. reported an emerging co-immobilization approach using *Spy*-tag and *Spy*-catcher fusion enzymes [32]. However, hydrogels self-assembled from free enzymes alone are mechanically fragile, which limit the operation strength and flow rate of continuous reactions. In comparison, immobilized *Kp*ADH Mu-S5 and *Bm*GDH maintained excellent catalytic activity and operational stability under a 5 min^{-1} dilution

rate during the first 3 days of the reaction. In a study by Dall'Oglio and coworkers, KRED1-Pglu and GDH were covalently bound to aldehyde activated agarose [31]. Although the stability and solvent tolerance were improved, alkaline operating conditions (pH⩾10) pose a challenge to the catalytic activity of enzymes. For example, Tt-ADH2 and formate dehydrogenase (FDH) had to be immobilized by covalent binding and ionic adsorption, respectively, due to the inactivation of FDH after aldehyde immobilization [35]. In our study, ADH and GDH were both coordination bound to Ni-NTA Cerose, and over 60% of catalytic activity could be maintained under near-neutral conditions (pH 7.5). Using commercially available enzyme membrane reactor, (*R*)-2-octanol could be continuously synthesized by co-immobilized *Lb*ADH and GDH, and produced a fairly high STY of 454 g/(L·d). Additionally, product separation and cofactor recycling were achieved by supercritical carbon dioxide ($scCO_2$) extraction [41] (**Table 2**).

In our study, the macroporous resin adsorption strategy with low equipment requirements was facilely used for product recovery, and in the subsequent resin extraction step, much less organic solvent was used than in traditional liquid-liquid extractions. Additionally, emulsification caused by proteins in free-enzyme systems was completely avoided, and a satisfactory yield was obtained by the simple operations of soaking and rotary evaporation.

Conclusions

Continuous flow biocatalysis can improve the overall reaction process by protecting

fragile enzymes from mechanical stirring or agitation, as well as simplifying the downstream product isolation and treatment. Herein, a 6×His-tag fused Mu-S5 and *Bm*GDH were co-immobilized on Ni-NTA Cerose to construct a PBR for continuous asymmetric synthesis of (*S*)-CPMA. As a support material for enzyme immobilization, the commercially available Ni-NTA Cerose is recyclable in process operation, Furthermore, the D101 macroporous resin column was used after the PBR to adsorb the (*S*)-CPMA product specifically, and recycling and reuse of the reaction solution containing hydrophilic $NADP^+$/NADPH was easily achieved. During 400 min of flow reaction, a 4 L initial reaction solution could be recycled up to 6 times, demonstrating the feasibility of reducing the cost of cofactors. Additionally, the (*S*)-CPMA product was enriched on the D101 resin and could be separated conveniently and effectively by soaking in ethyl acetate. In summary, the designed continuous biocatalytic process using coupled PBR and *in situ* product recovery could be potentially applied in preparation of chiral alcohols. This continuous flow biocatalysis system is especially suitable for enzymatic reactions involving cofactor recycling and substrate/product inhibitory issues.

Acknowledgements

This work was supported by National Key R&D Program [2018YFA0901700], National Natural Science Foundation of China [21907040, 21776112, 22077054], China Postdoctoral Science Foundation [2019M651703], National First-Class Discipline Program of Light Industry Technology and Engineering [LITE2018-07],

and the Program of Introducing Talents of Discipline to Universities [111-2-06].

Authors' contributions

Jieyu Zhou: Conceptualization, Investigation, Methodology, Writing-original draft. Yanfei Wu: Data curation. Qingye Zhang: Data curation, Formal analysis. Guochao Xu: Writing-review & editing. Ye Ni: Supervision, Writing-review & editing, Project administration, Funding acquisition.

Compliance with Ethical Standards

Competing Interests The authors declare that they have no known competing financial interests or personal relationships that could have appeared to influence the work reported in this paper

Supplementary

Supplementary material related to this article can be found in the online version.

References

1. Britton, J., Majumdar, S. and Weiss, G.A. (2018) Chem. Soc. Rev. 47, 5891-5918.
2. Adamo, A., Beingessner, R.L., Behnam, M., Chen, J., Jamison, T.F., Jensen, K.F., Monbaliu, J.M., Myerson, A.S., Revalor, E.M., Snead, D.R., Stelzer, T., Weeranoppanant, N., Wong, S.Y. and Zhang, P. (2016) Science 352, 54-61.
3. Webb, D. and Jamison, T.F. (2010) Chem. Sci. 1, 675-680.
4. Cuong, N.P., Lee, W., Oh, I., Thuy, N.M., Kim, D., Park, J. and Park, K. (2016) Process Biochem. 51, 282-287.
5. Cimporescu, A., Todea, A., Badea, V., Paul, C. and Peter, F. (2016) Process Biochem. 51, 2076-2083.
6. Jia, C., Wang, H., Zhang, W., Zhang, X. and Feng, B. (2018) Process Biochem. 66, 28-32.
7. de Oliveira Lopes, R., Ribeiro, J.B., Silva De Miranda, A., Vieira Da Silva, G.V., Miranda, L.S.M., Ramos Leal, I.C. and Mendonça Alves De Souza, R.O. (2014). Tetrahedron 70, 3239-3242.
8. Tamborini, L., Romano, D., Pinto, A., Contente, M., Iannuzzi, M.C., Conti, P. and Molinari, F. (2013). Tetrahedron Lett. 54, 6090-6093.
9. J. Döbber, T.G.H.O. (2018). Green Chem. 20, 544-552.
10. Xiao, M., Qi, C. and Obbard, J.P. (2011) Bioenergy 3, 293-298.
11. Tan, A.W., Fischbach, M., Huebner, H., Buchholz, R., Hummel, W., Daussmann, T., Wandrey, C. and Liese, A. (2006). Appl. Microbiol. Biotechnol. 71, 289-93.

12. Thompson, M.P., Peñafiel, I., Cosgrove, S.C. and Turner, N.J. (2018). Org. Process Res. Dev. 23, 9-18.
13. Li, F., Zheng, Y., Li, H., Chen, F., Yu, H. and Xu, J. (2019). Tetrahedron 75, 1706-1710.
14. Orrego, A.H., López-Gallego, F., Espaillat, A., Cava, F., M., J. and A, G.A.A.J. (2018). ChemCatChem 10, 3002-3011.
15. García-García, P., Rocha-Martin, J., Fernandez-Lorente, G. and Guisan, J.M. (2018) Enzyme Microb. Tech. 115, 73-80.
16. Arana-Pena, S., Carballares, D., Morellon-Sterlling, R., Berenguer-Murcia, A., Alcantara, A.R., Rodrigues, R.C. and Fernandez-Lafuente, R. (2020). Biotechnol. Adv. 107584.
17. Rocha-Martín, J., Rivas, B.D.L., Muñoz, R., Guisán, J.M. and López-Gallego, F. (2012). ChemCatChem 4, 1279-1288.
18. Trobo-Maseda, L., Orrego, A.H., Guisan, J.M. and Rocha-Martin, J. (2020). Int. J. Biol. Macromol. 157, 510–521.
19. Hearon, J.Z., Sundberg, L., and MalmstrOm, B.G. (1975). Nature 258, 598-599.
20. Planchestainer, M., Contente, M.L., Cassidy, J., Molinari, F., Tamborini, L. and Paradisi, F. (2017) Green Chem. 19, 372-375.
21. Liu, J., Pang, B.Q.W., Adams, J.P., Snajdrova, R. and Li, Z. (2017). ChemCatChem 9, 425-431.
22. Vahidi, A.K., Yang, Y., Ngo, T.P.N. and Li, Z. (2015). ACS Catal. 5, 3157-3161.
23. Yang, J., Ni, K., Wei, D. and Ren, Y. (2015). Biotechnol. Bioproc. E. 20, 901-

907.

24. Engelmark Cassimjee, K., Kadow, M., Wikmark, Y., Svedendahl Humble, M., Rothstein, M.L., Rothstein, D.M. and Bäckvall, J.E. (2014). Chem. Commun. 50, 9134.
25. Ueda, E.K.M., Gout, P.W. and Morganti, L. (2003). J. Chromatogr. A. 988, 1-23.
26. Chou, Y., Ko, C., Chen, L.O. and Shaw, C.Y. (2015). Molecules 20, 3744-3757.
27. Böhmer, W., Knaus, T. and Mutti, F.G. (2018). ChemCatChem 10, 731-735.
28. Melchers, K., Herrmann, L., Mauch, F., Bayle, D., Heuermann, D., Weitzenegger, T., Schuhmacher, A., Sachs, G., Haas, R., Bode, G., Bensch, K. and Schäfer, K.P. (1998). Acta. Physiol. Scand. Suppl. 643, 123-135.
29. Melchers, K., Weitzenegger, T., Buhmann, A., Steinhilber, W., Sachs, G. and Schafer, K.P. (1996). J. Biol. Chem. 271, 446-57.
30. Hou, J., Jin, Q., Du, J., Li, Q., Yuan, Q. and Yang, J. (2014). Bioproc. Biosyst. Eng. 37, 857-864.
31. Dall'Oglio, F., Contente, M.L., Conti, P., Molinari, F., Monfredi, D., Pinto, A., Romano, D., Ubiali, D., Tamborini, L. and Serra, I. (2017). Catal. Commun. 93, 29-32.
32. Peschke, T., Bitterwolf, P., Gallus, S., Hu, Y., Oelschlaeger, C., Willenbacher, N., Rabe, K.S. and Niemeyer, C.M. (2018). Angew. Chem., int. Edit. 57, 17028-17032.
33. Fassouane, A., Laval, J.M., Moiroux, J. and Bourdillon, C. (1990). Biotechnol. Bioeng. 35, 935-939.

579 34. Ruinatscha, R., Buehler, K. and Schmid, A. (2014). J. Mol. Catal. B-Enzym. 103,
580 100-105.
581 35. Velasco-Lozano, S., Benítez-Mateos, A.I. and López-Gallego, F. (2017). Angew.
582 Chem., int. Edit. 56, 771-775.
583 36. Benítez-Mateos, A.I., San Sebastian, E., Ríos-Lombardía, N., Morís, F.,
584 González-Sabín, J. and López-Gallego, F. (2017). Chem-Eur. J. 23, 16843-16852.
585 37. Zhou, J., Xu, G., Han, R., Dong, J., Zhang, W., Zhang, R. and Ni, Y. (2016).
586 Catal. Sci. Technol. 6, 6320-6327.
587 38. Zhou, J., Wang, Y., Xu, G., Wu, L., Han, R., Schwaneberg, U., Rao, Y., Zhao,
588 Y., Zhou, J. and Ni, Y. (2018). J. Am. Chem. Soc. 140, 12645-12654.
589 39. Ni, Y., Zhou, J. and Sun, Z. (2012). Process Biochem. 47, 1042-1048.
590 40. Gaberc-Porekar, V. and Menart, V. (2001). J. Biochem. Biophys. Methods 49,
591 335–360.
592 41. Kohlmann, C., Leuchs, S., Greiner, L. and Leitnera, W. (2011). Green Chem. 13,
593 1430-1437.
594

595 **Table and Figure Legends**

596 **Table 1.** Comparison of properties of D101 and XDA-1 resins.

597 **Table 2.** Comparison of asymmetric reductions catalyzed by various alcohol
598 dehydrogenases (ADHs) and glucose dehydrogenases (GDHs)/formate
599 dehydrogenases (FDHs) in flow reactions.

600 **Fig. 1.** Continuous biosynthesis of (*S*)-(4-chlorophenyl)-(pyridin-2-yl) methanol (*S*-
601 CPMA) with immobilized Mu-S5 and *Bm*GDH and *in situ* product recovery.

602 **Fig. 2.** Effect of metal ions on catalytic activity of Mu-S5 (A). Effect of dilution ratio
603 on conversion ratio of Ni-and Mn-functionalized porous ceramic/agarose composite
604 beads (Cerose) immobilized enzymes (B).

605 **Fig. 3.** SDS-PAGE of recombinant Mu-S5 fused with Heli-Tag (A) or 6×His Tag (B)
606 eluted at different Imidazole Concentrations. (A) M: protein ladder; lane 1:
607 supernatant of crude Heli-tag fused Mu-S5; lane 2: sediment of crude Heli-tag fused
608 Mu-S5; lane 3: Flow-through of crude Heli-tag fused Mu-S5; lane 4-7: eluent from
609 washing Heli-tag fused Mu-S5 with 20, 50, 100 and 300 mM imidazole, respectively;
610 (B) M: protein ladder; lane 1: supernatant of crude 6×His-tag fused Mu-S5; lane 2:
611 sediment of crude 6×His-tag fused Mu-S5; lane 3: Flow-through of crude 6×His-tag
612 fused Mu-S5; lane 4-7: eluent from washing 6×His-tag fused Mu-S5 with 20, 50, 100
613 and 300 mM imidazole, respectively.

614 **Fig. 4.** Optimization of reaction catalyzed by immobilized Mu-S5 and *Bm*GDH. (A)
615 pH; (B) temperature; (C) ratio of Mu-S5 and *Bm*GDH; (D) co-solvent; (E) flow rate
616 optimum of (4-chlorophenyl)(pyridine-2-yl)ketone (CPMK) in a 10-mL Ni-

617 functionalized porous ceramic/agarose composite beads (Ni−NTA Cerose) packed bed
618 reactor.
619 **Fig. 5.** Continuous production of (*S*)-(4-chlorophenyl)-(pyridin-2-yl) methanol (*S*-
620 CPMA) in a 10-mL packed bed reactor.
621

622 **Table 1.**

Resin	Constituent materials	Average aperture size (nm)	Specific surface area (m^2/g)	Static adsorption rate (%)	Desorption rate (%)
D101	Polystyrene	25−28	480−520	88.1±0.13	96.1±0.22
XDA-1	Polyacrylic acid	85−89	1000−1100	91.3±0.08	82.7±0.31

623

Table 2.

	This study	Peschke et al. [32]	Dall'Oglio et al.[31]	Kohlmann et al.[41]	Velasco-Lozano et al [35]
Ketone reductase	Mu-S5 from *Kluyveromyces polyspora*	*Lb*ADH from *Lactobacillus brevis*	KRED1-Pglu from *Pichia glucozyma*	*Lb*ADH from *Lactobacillus brevis*	Tt-ADH2 from *Thermus thermophilus*
Cofactor recycling	GDH	GDH	GDH	GDH	FDH
Immobilized strategy	IMAC	Self-assembling;	Covalent binding	Interception by semi-permeable membrane	Covalent binding & ionic adsorption
Support material	Cerose	Hydrogel	Aldehyde activated agarose	Enzyme membrane reactor	Aldehyde activated agarose & polyethyleneimine agarose
Substrate	CPMK	5-nitrononane-2,8-dione	1-phenylpropane-1,2-dione	octan-2-one	2,2,2-trifluoro-1-phenylethanone
Conc.(mM)	10	5.0	3.0	6.0	5.0
Reactor volume (mL)	10	0.15	0.90	16	1.2
Flow rate (mL/min)	5.0	0.010	0.050	0.10	0.050
SYT (g/(L·d))	1560	≈100	4.4–81.5	454.5	62.7
In situ product recovery	Macroporous resins adsprption	No	No	scCO2 extraction.	No

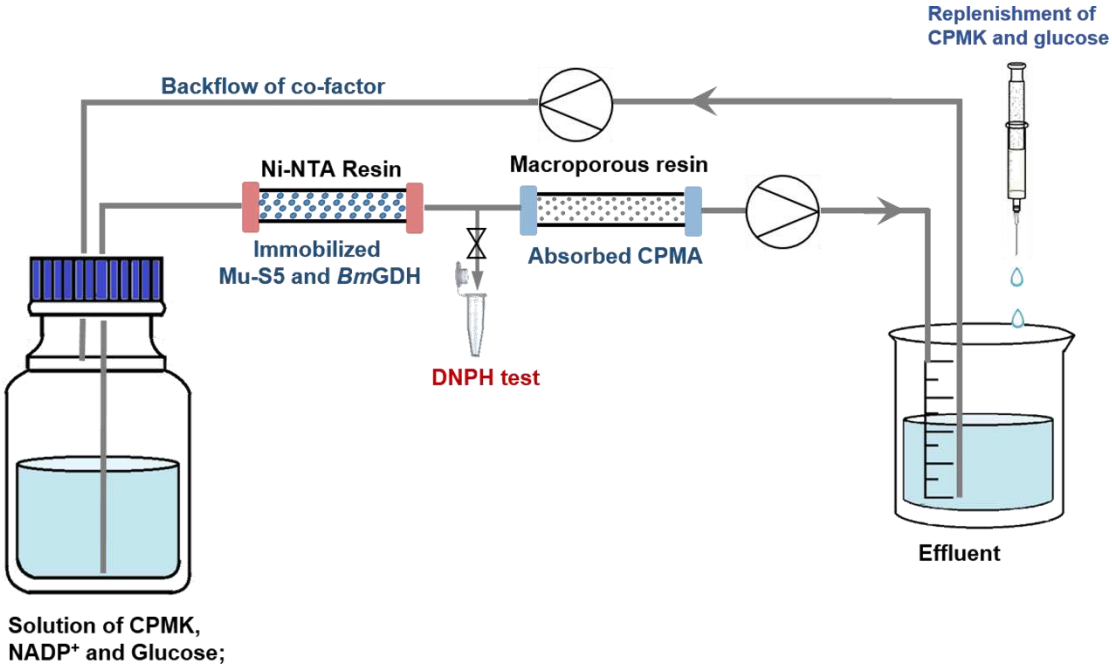
Replenishment of
CPMK and glucose
Backflow of co-factor
Ni-NTA Resin
Macroporous resin
Immobilized
Mu-S5 and BmGDH
Absorbed CPMA
DNPH test
Effluent
Solution of CPMK,
NADP+ and Glucose;

Fig. 1.

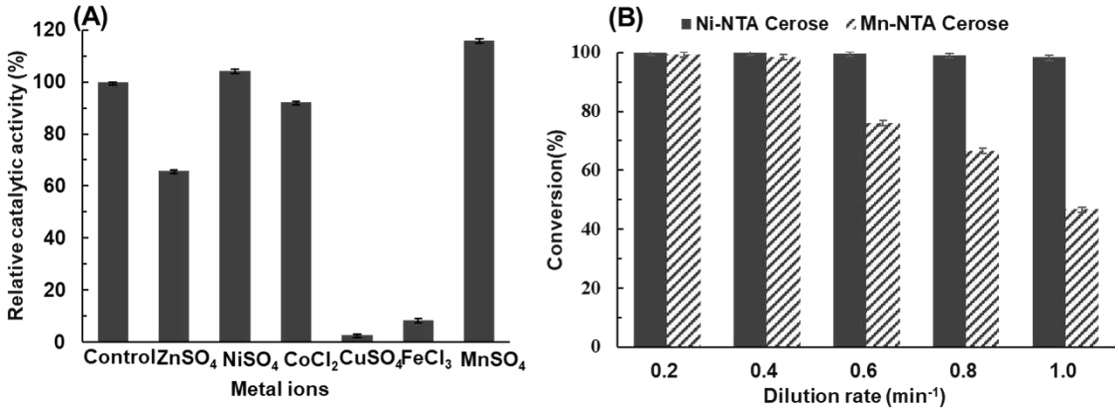
(A)
Relative catalytic activity (%)
120
100
80
60
40
20
0
Control
ZnSO4
NiSO4
CoCl2
CuSO4
FeCl3
MnSO4
Metal ions
(B)
Ni-NTA Cerose
Mn-NTA Cerose
Conversion(%)
100
80
60
40
20
0
0.2
0.4
0.6
0.8
1.0
Dilution rate (min-1)

628

629 **Fig. 2.**

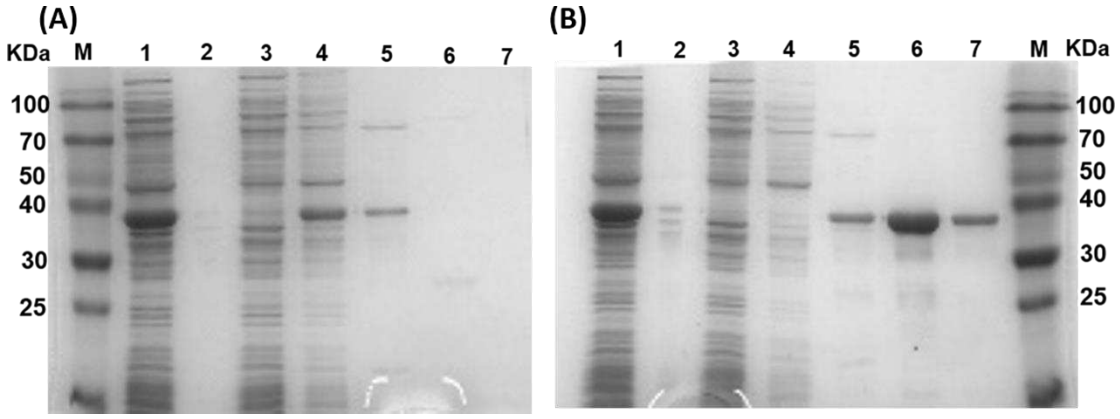
(A)
KDa
M
1
2
3
4
5
6
7
100
70
50
40
30
25
(B)
1
2
3
4
5
6
7
M
KDa
100
70
50
40
30
25

630

631 **Fig. 3.**

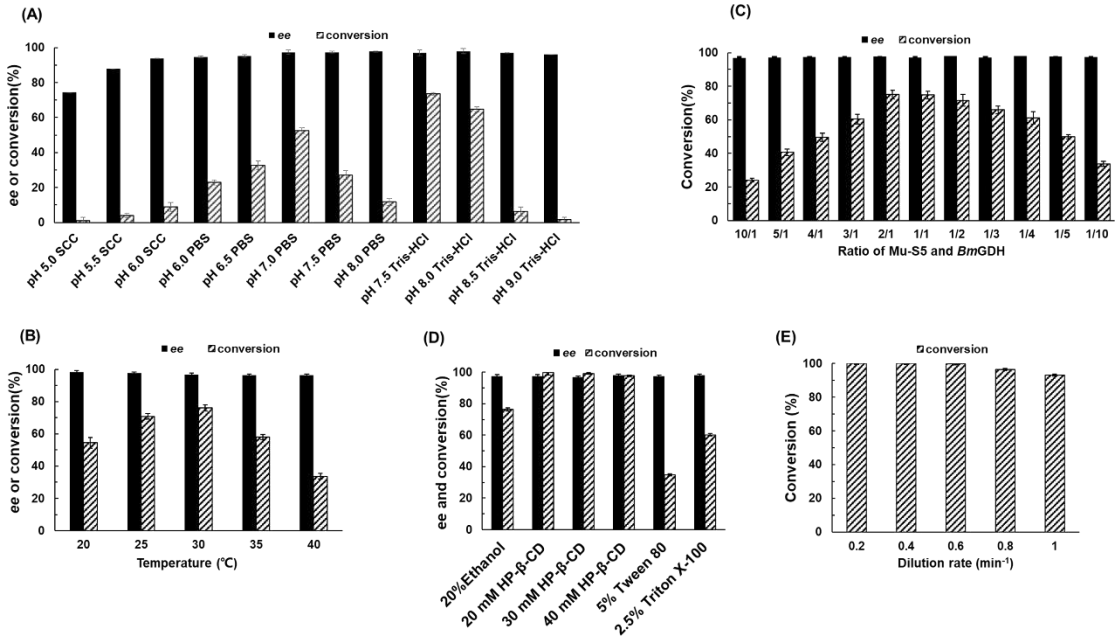
(A)
ee
conversion
ee or conversion(%)
pH 5.0 SCC
pH 5.5 SCC
pH 6.0 SCC
pH 6.0 PBS
pH 6.5 PBS
pH 7.0 PBS
pH 7.5 PBS
pH 8.0 PBS
pH 7.5 Tris-HCl
pH 8.0 Tris-HCl
pH 8.5 Tris-HCl
pH 9.0 Tris-HCl
(C)
Conversion(%)
10/1
5/1
4/1
3/1
2/1
1/1
1/2
1/3
1/4
1/5
1/10
Ratio of Mu-S5 and BmGDH
(B)
Temperature (℃)
(D)
ee and conversion(%)
20%Ethanol
20 mM HP-β-CD
30 mM HP-β-CD
40 mM HP-β-CD
5% Tween 80
2.5% Triton X-100
(E)
Conversion (%)
Dilution rate (min-1)

632

633 **Fig. 4.**

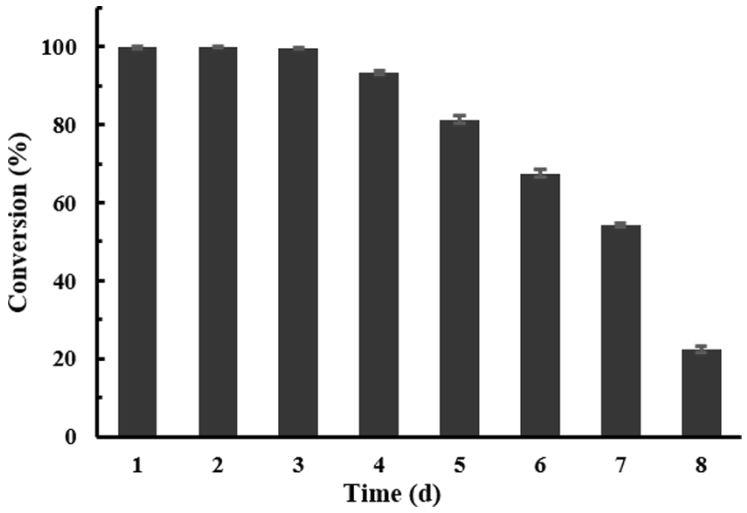

634

635 **Fig. 5**

Figures

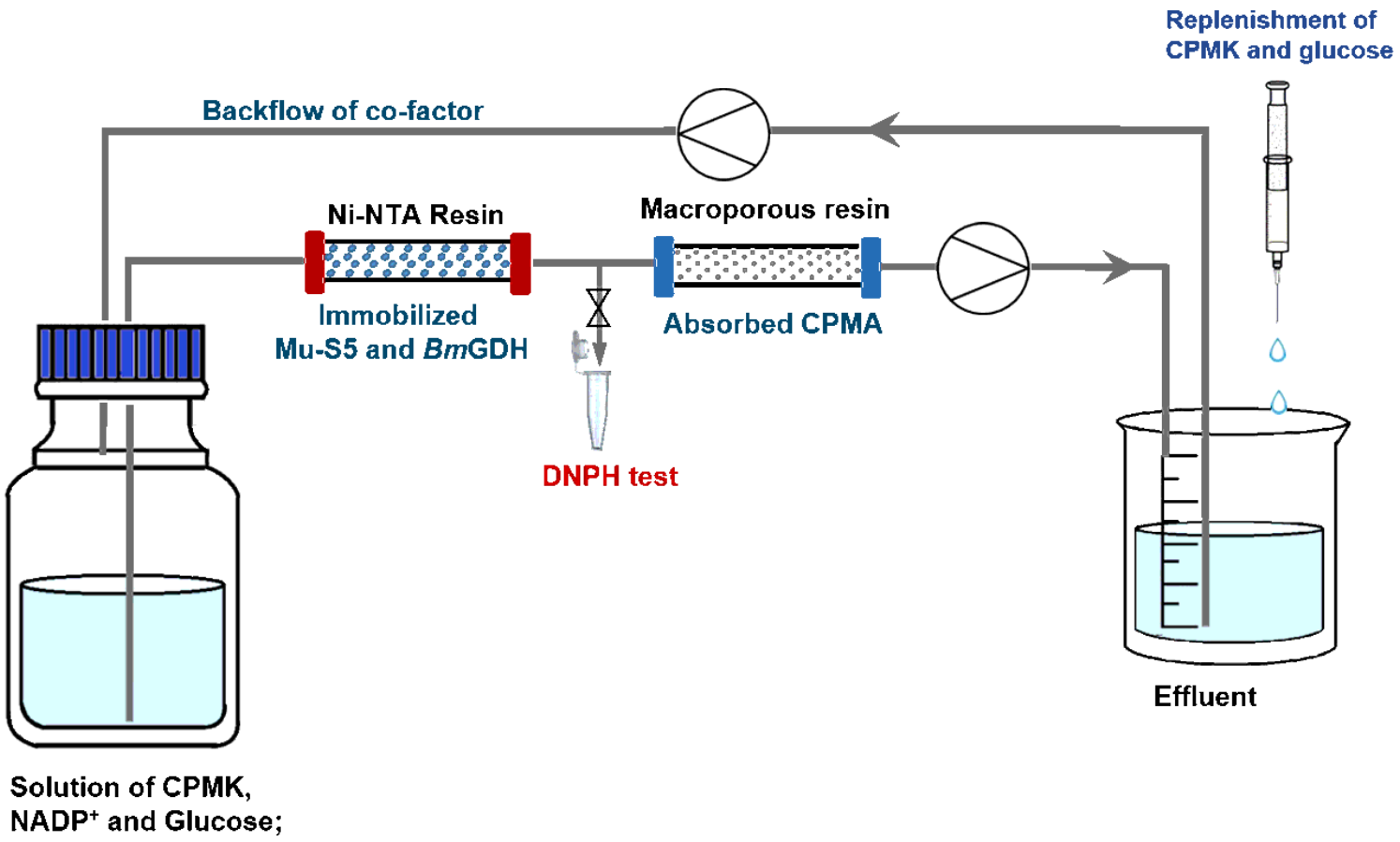

Figure 1

Continuous biosynthesis of (S)-(4-chlorophenyl)-(pyridin-2-yl) methanol (S-CPMA) with immobilized Mu-S5 and BmGDH and in situ product recovery.

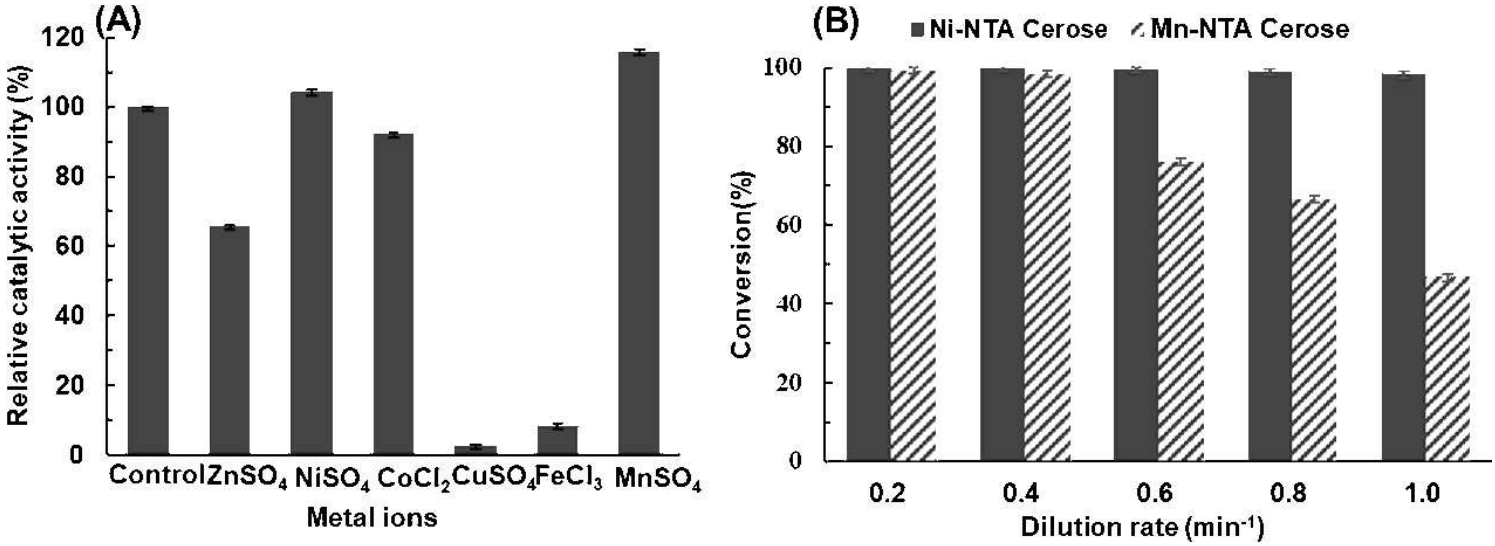

Figure 2

Effect of metal ions on catalytic activity of Mu-S5 (A). Effect of dilution ratio on conversion ratio of Ni- and Mn-functionalized porous ceramic/agarose composite beads (Cerose) immobilized enzymes (B).

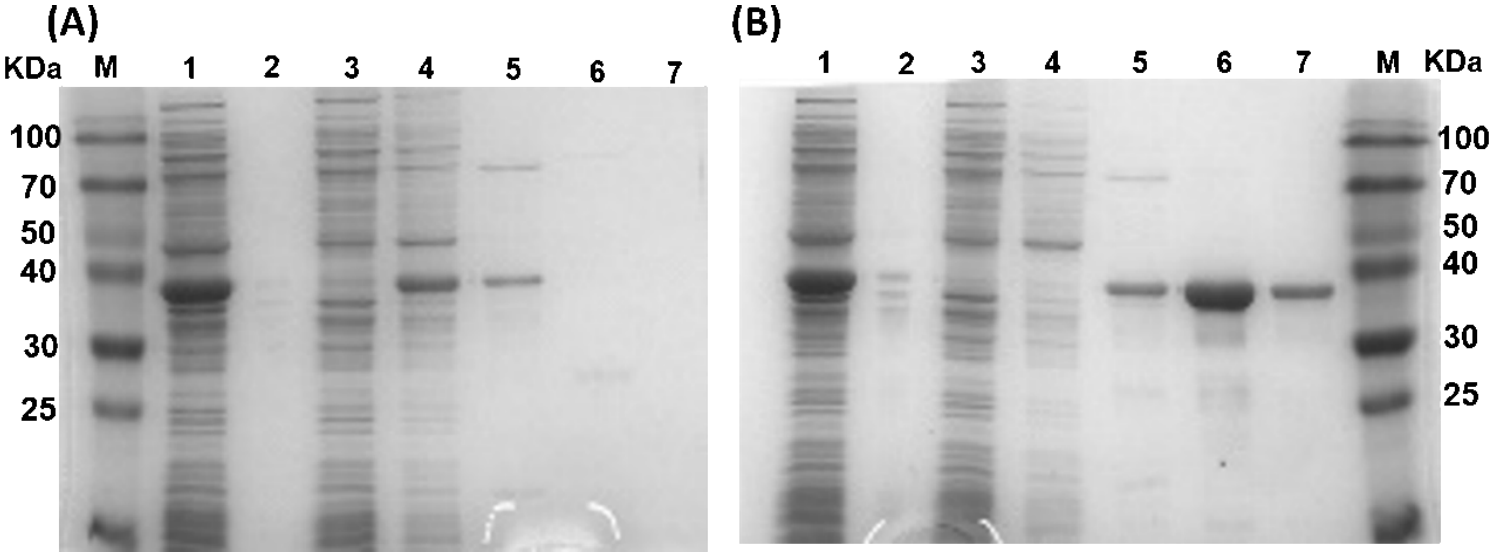

Figure 3

SDS-PAGE of recombinant Mu-S5 fused with Heli-Tag (A) or 6×His Tag (B) eluted at different Imidazole Concentrations. (A) M: protein ladder; lane 1: supernatant of crude Heli-tag fused Mu-S5; lane 2: sediment of crude Heli-tag fused Mu-S5; lane 3: Flow-through of crude Heli-tag fused Mu-S5; lane 4-7: eluent from washing Heli-tag fused Mu-S5 with 20, 50, 100 and 300 mM imidazole, respectively; (B) M: protein ladder; lane 1: supernatant of crude 6×His-tag fused Mu-S5; lane 2: sediment of crude 6×His-tag fused Mu-S5; lane 3: Flow-through of crude 6×His-tag fused Mu-S5; lane 4-7: eluent from washing 6×His-tag fused Mu-S5 with 20, 50, 100 and 300 mM imidazole, respectively.

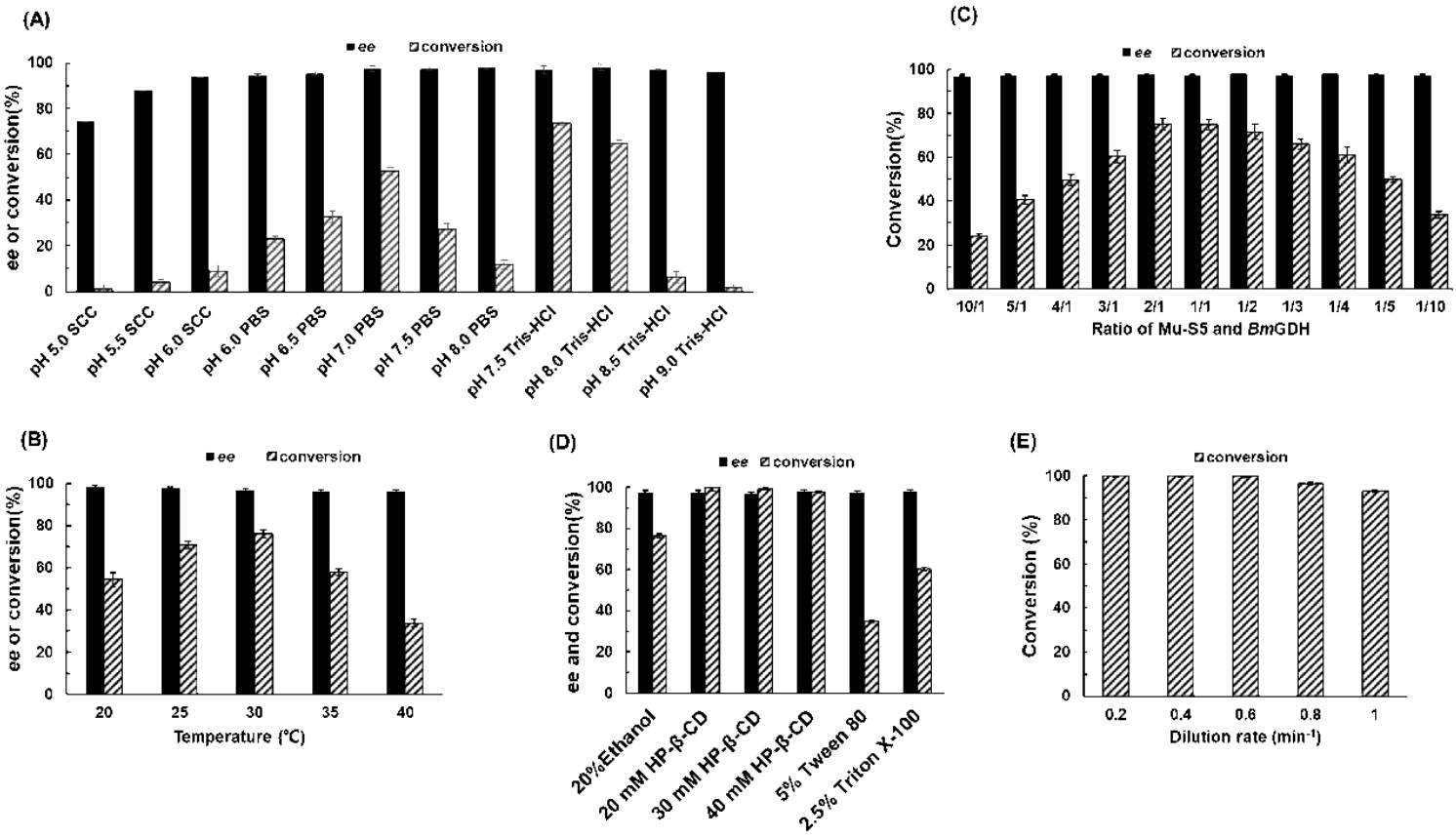

Figure 4

Optimization of reaction catalyzed by immobilized Mu-S5 and BmGDH. (A) pH; (B) temperature; (C) ratio of Mu-S5 and BmGDH; (D) co-solvent; (E) flow rate optimum of (4-chlorophenyl)(pyridine-2-yl)ketone (CPMK) in a 10-mL Ni-functionalized porous ceramic/agarose composite beads (Ni-NTA Cerose) packed bed reactor.

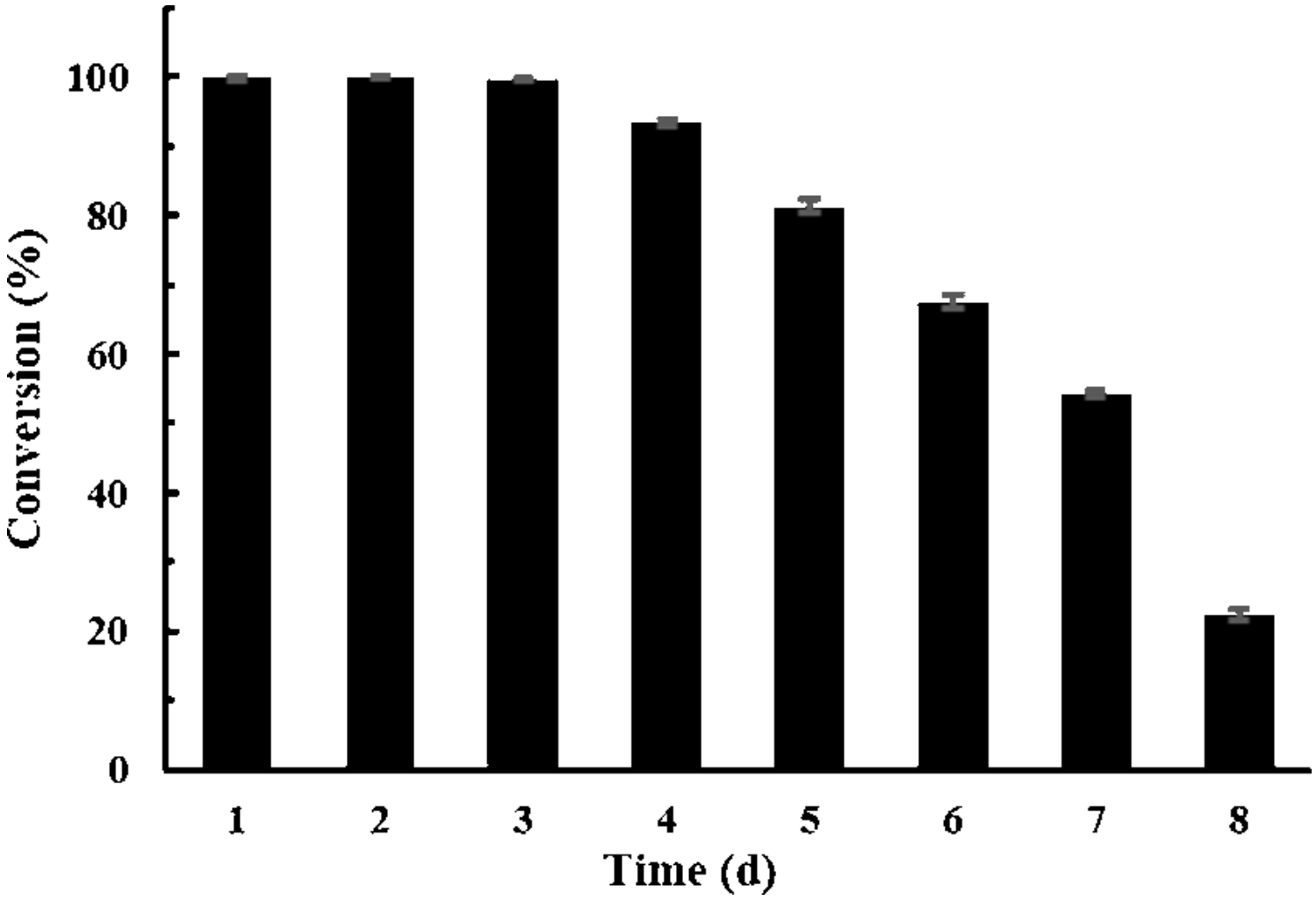

Figure 5

Continuous production of (S)-(4-chlorophenyl)-(pyridin-2-yl) methanol (S-CPMA) in a 10-mL packed bed reactor.

Supplementary Files

This is a list of supplementary files associated with this preprint. Click to download.

- 2021.2.5supportinginformation.docx